Pixelated liquid perovskite array for high-sensitivity and high-resolution X-ray imaging scintillation screens

Mingzhu Hu[1,2,3,§], Yumeng Wang[1,2,§], Shengpeng Hu[1,2,§], Zongpeng Wang[4], Bi Du[4], Yanjun Peng[1,2], Jiawei Yang[1,2], Yunjie Shi[1], Dongdong Chen[1,2], Xi Chen[1,2], Ziwen Zhuang[1], Zhixun Wang[6], Xi Chen[1,5], Jiecheng Yang[7,8], Yongshuai Ge[7,8], Eyu Wang[9], Quan Wen[9], Shuang Xiao[10], Ming Ma[1,5], Weimin Li[1,5], Jie Zhang[1,5], De Ning[1,5*], Lei Wei[6*], Chunlei Yang[1,5*] and Ming Chen[1,5*]

[1]Shenzhen Institute of Advanced Technology, Chinese Academy of Sciences, Shenzhen 518055, People's Republic of China

[2]Department of Nano Science and Technology Institute, University of Science and Technology of China, Suzhou 215123, People's Republic of China

[3]School of Microelectronics, University of Science and Technology of China, Hefei 230026, People's Republic of China

[4]Shenzhen Angell Technology Co. Ltd., Shenzhen 518057, People's Republic of China

[5]University of Chinese Academy of Sciences, Beijing 100049, People's Republic of China

[6]School of Electrical and Electronic Engineering, Nanyang Technological University, 50 Nanyang Avenue, 639798, Singapore

[7]Paul C Lauterbur Research Center for Biomedical Imaging, Shenzhen Institute of Advanced Technology, Chinese Academy of Sciences, Shenzhen, Guangdong 518055, China

[8]Research Center for Medical Artificial Intelligence, Shenzhen Institute of Advanced Technology, Chinese Academy of Sciences, Shenzhen, Guangdong 518055, China

[9]Seamark Opoticelectronic Technology (Shenzhen) Co. Ltd, Shenzhen, 518103, People's Republic of China

[10]Shenzhen Key Laboratory of Ultraintense Laser and Advanced Material Technology, Center for Advanced Material Diagnostic Technology, and College of Engineering Physics, Shenzhen Technology University, Shenzhen 518118, China

*Corresponding author: de.ning@siat.ac.cn; wei.lei@ntu.edu.sg; cl.yang@siat.ac.cn; ming.chen2@siat.ac.cn;

[§]These authors contributed equally to this work

Keywords: perovskite, X-ray imaging, liquid scintillator screen, pixelated, high sensitivity.

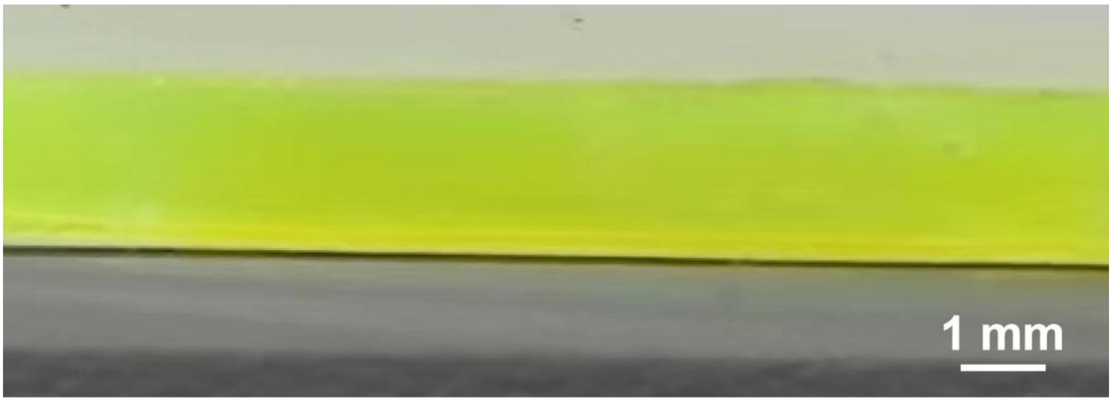

Figure S1 Cross-sectional image of the pixelated $CsPbBr_3$/PPO liquid scintillator arrays

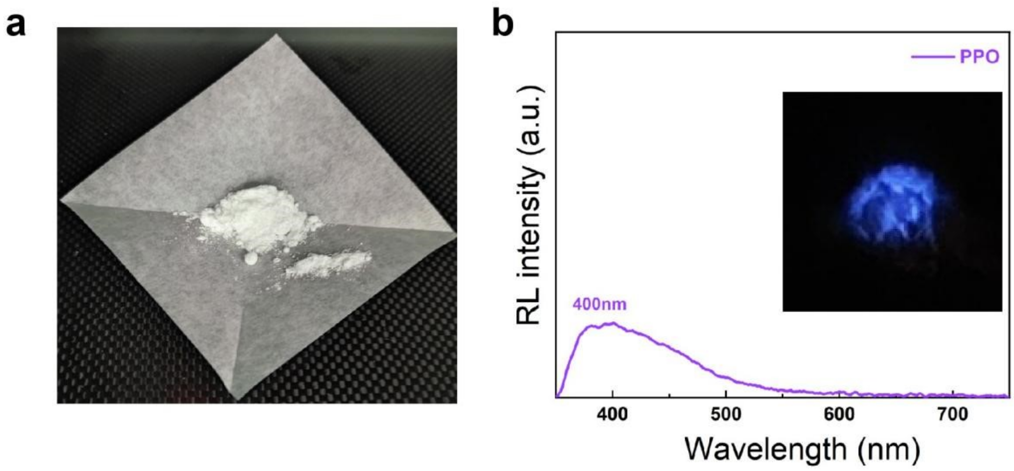

Figure S2 (a) Photograph of the PPO powder. (b) RL spectra of PPO powder. Inset is the image of PPO under X-ray irradiation.

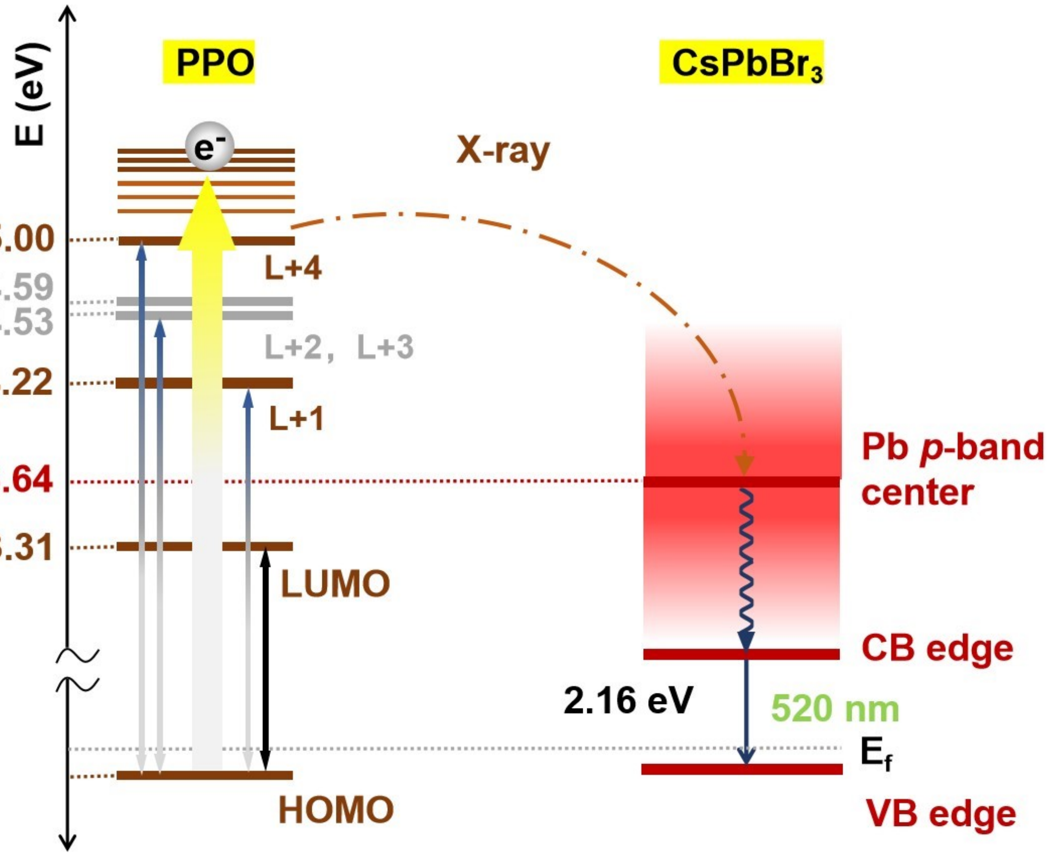

Figure S3 Energy level alignment for the proposed mechanism of enhanced RL in the $CsPbBr_3$ QDs/PPO scintillator.

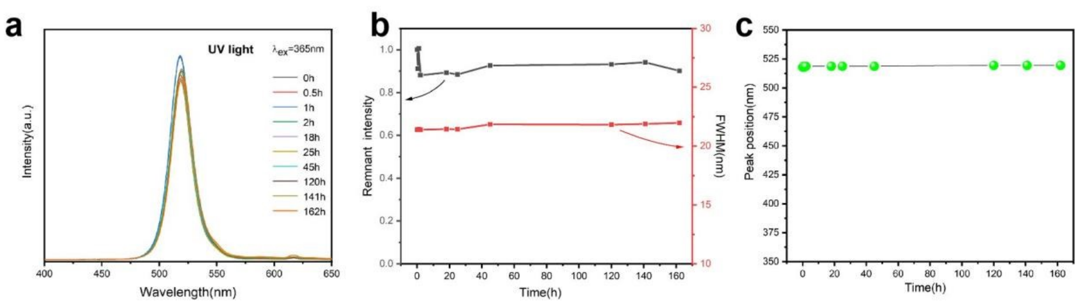

Figure S4 (a) PL spectrum of $CsPbBr_3$ QDs/PPO LSS in ambient atmosphere. (b) PL peak intensity and FWHM of $CsPbBr_3$ QDs/PPO LSS extracted from (a). (c) PL peak position of $CsPbBr_3$ QDs/PPO LSS extracted from a).

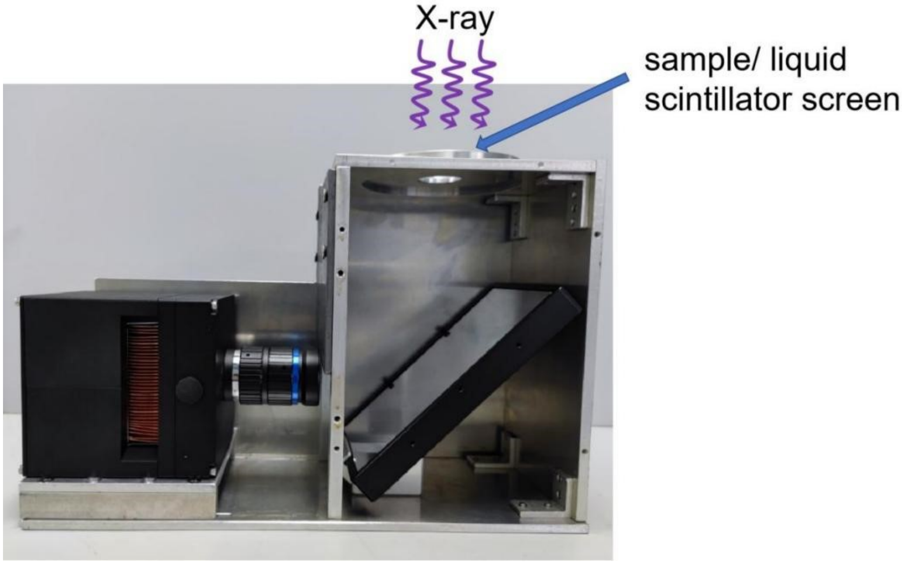

Figure S5 X-ray imaging optical system.

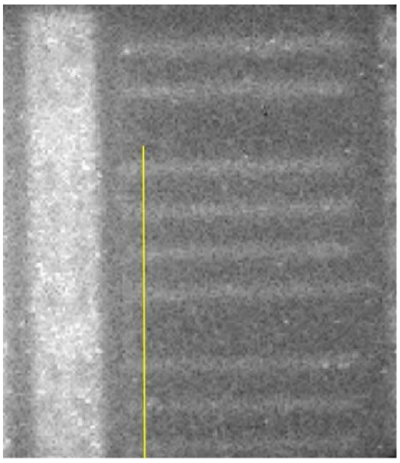

Figure S6. X-ray imaging of the standard line-pair card by the pixelated $CsPbBr_3$/PPO LSS.

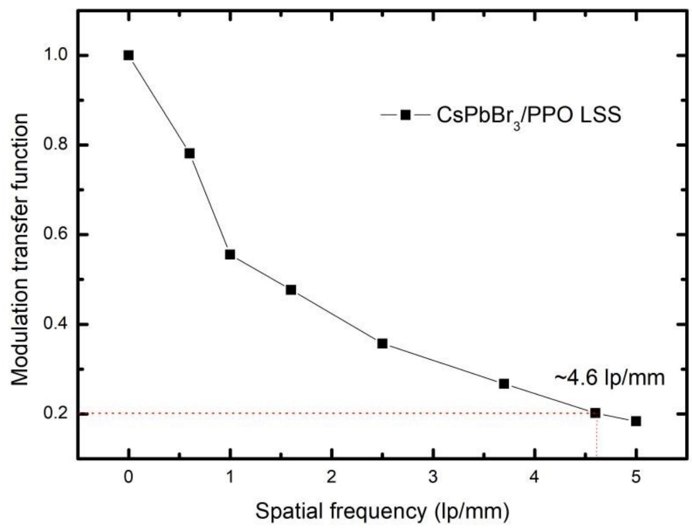

Figure S7. Modulation transfer function (MTF) of $CsPbBr_3$ QDs/PPO LSS

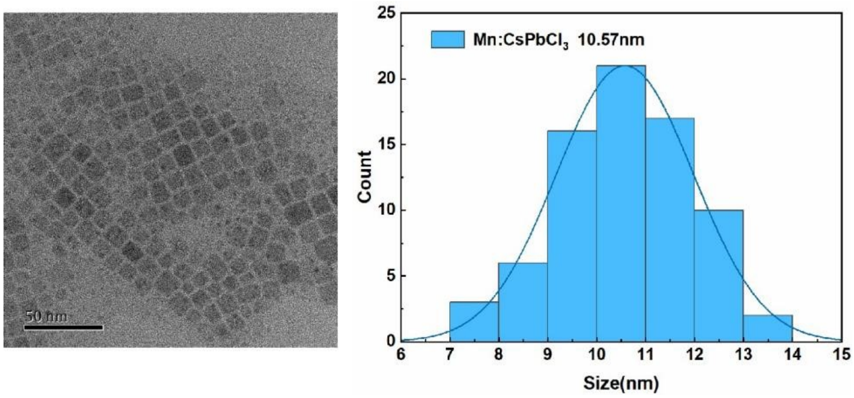

Figure S8 TEM image and particle size distribution of the Mn:$CsPbCl_3$ QDs

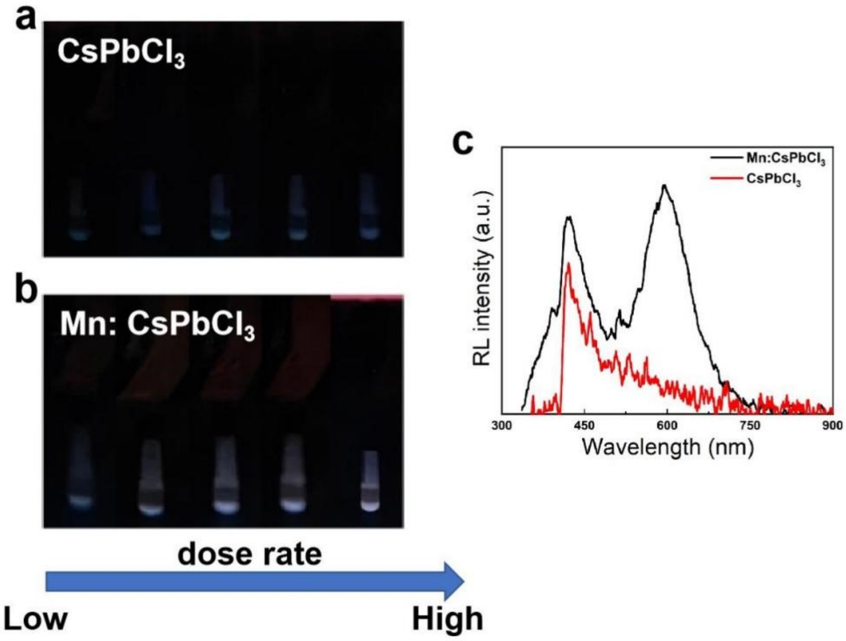

Figure S9 (a-b)X-ray image of $CsPbCl_3$ QDs and Mn: $CsPbCl_3$ QDs under X-ray irradiation with different dose rate, respectively. (c) RL spectra of $CsPbCl_3$ QDs and Mn: $CsPbCl_3$ QDs.

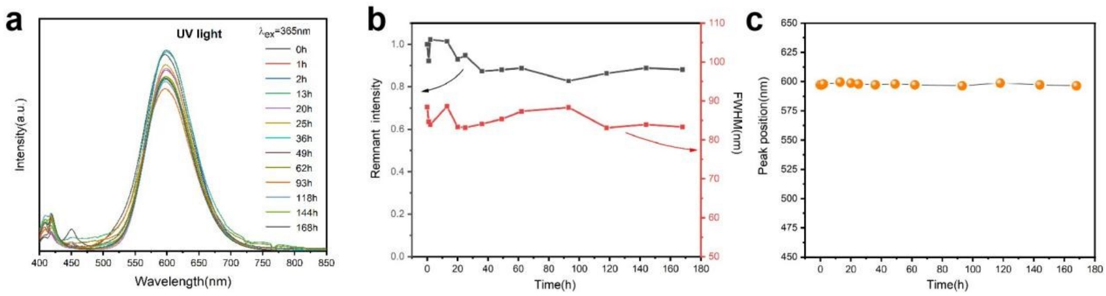

Figure S10 (a) PL spectrum of Mn: $CsPbCl_3$ QDs/PPO LSS in ambient atmosphere. (b) PL peak intensity and FWHM of Mn: $CsPbCl_3$ QDs/PPO LSS extracted from (a). (c) PL peak position of Mn: $CsPbCl_3$ QDs/PPO LSS extracted from (a).

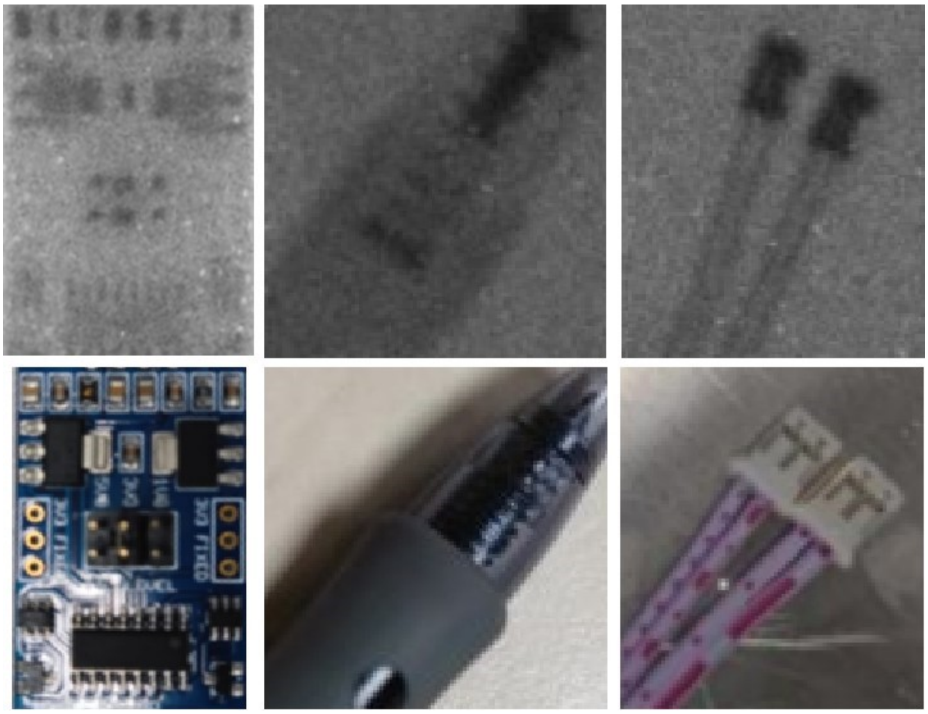

Figure S11. X-ray images and photographs of circuit board, ball-point pen and leadwire using Mn: $CsPbCl_3$ QDs/PPO LSS.

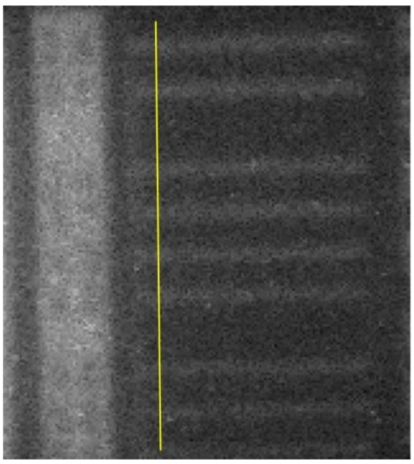

Figure S12 X-ray imaging of the standard line-pair card by the pixelated Mn: $CsPbCl_3$/PPO LSS.

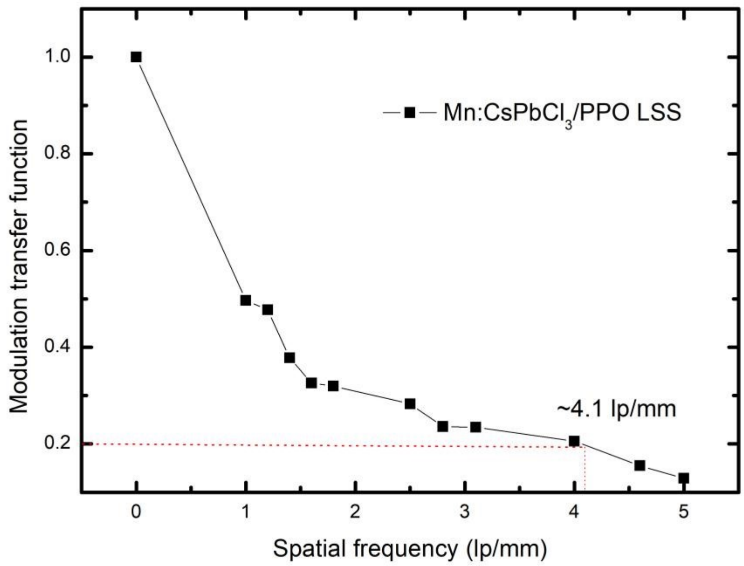

Figure S13. MTF of Mn:$CsPbCl_3$ QDs/PPO LSS

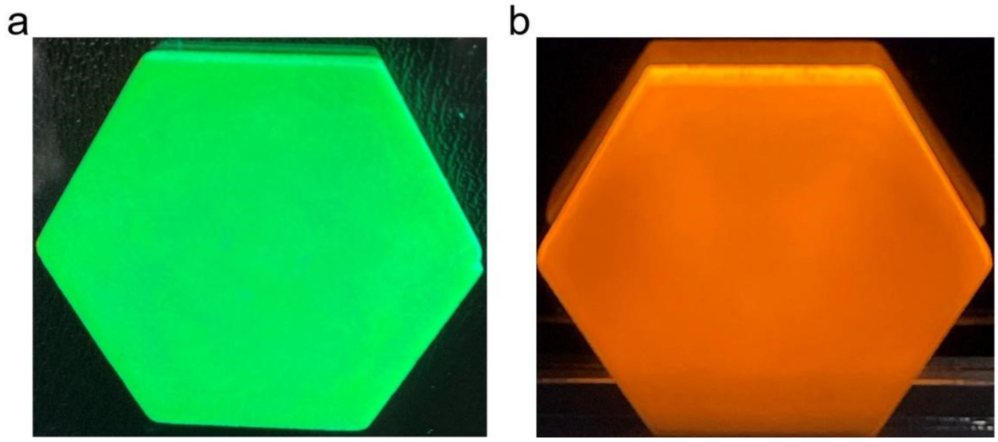

Figure S14. (a-b) Optical image of the pixelated $CsPbBr_3$/PPO and Mn:$CsPbCl_3$ QDs/PPO liquid scintillator arrays under UV light excitation after the repeated filling/packaging process, respectively.

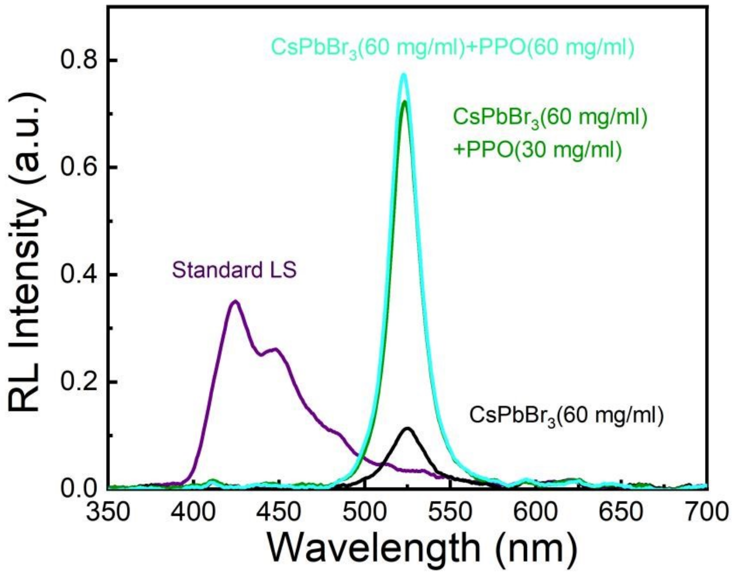

Figure S15. RL spectra of standard liquid scintillator (PPO+POPOP+toluene), $CsPbBr_3$(60 mg/ml), $CsPbBr_3$(60 mg/ml)+PPO (30 mg/ml) and $CsPbBr_3$(60 mg/ml)+PPO (60 mg/ml), measured at 90 kV, 89 uA

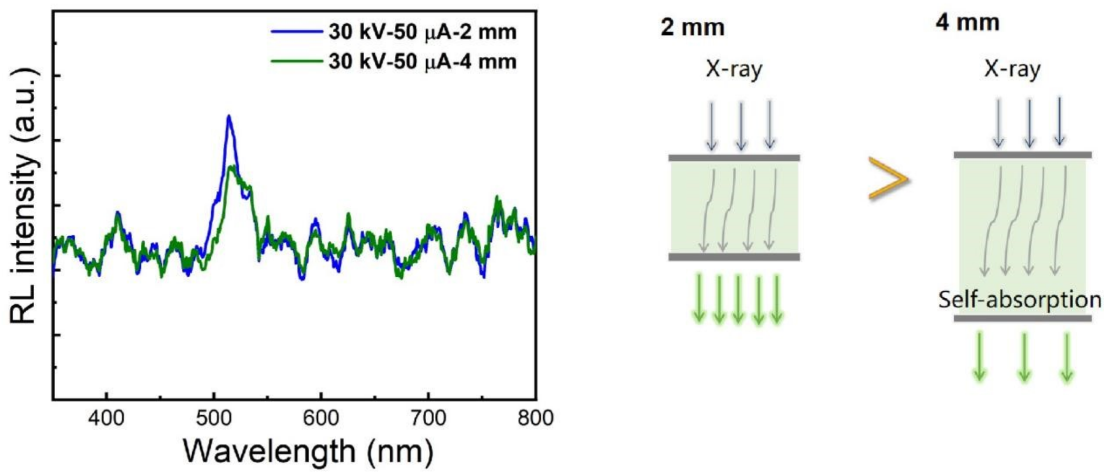

Figure S16 RL spectra of $CsPbBr_3$ QDs/PPO LSS with 2 mm and 4 mm thickness (30 kV-50 μA).

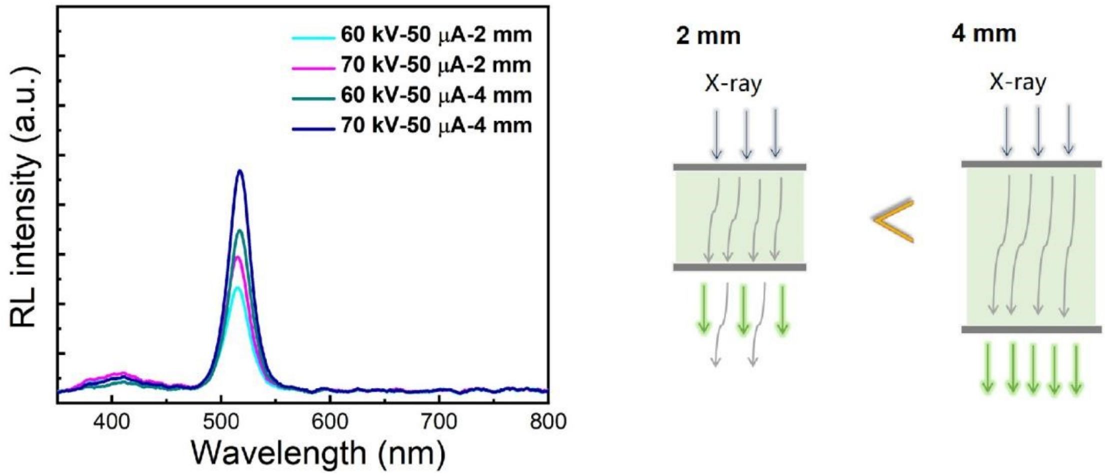

Figure S17 RL spectra of $CsPbBr_3$ QDs/PPO LSS with 2 mm and 4 mm thickness (60 kV-50 μA and 70 kV-50 μA).

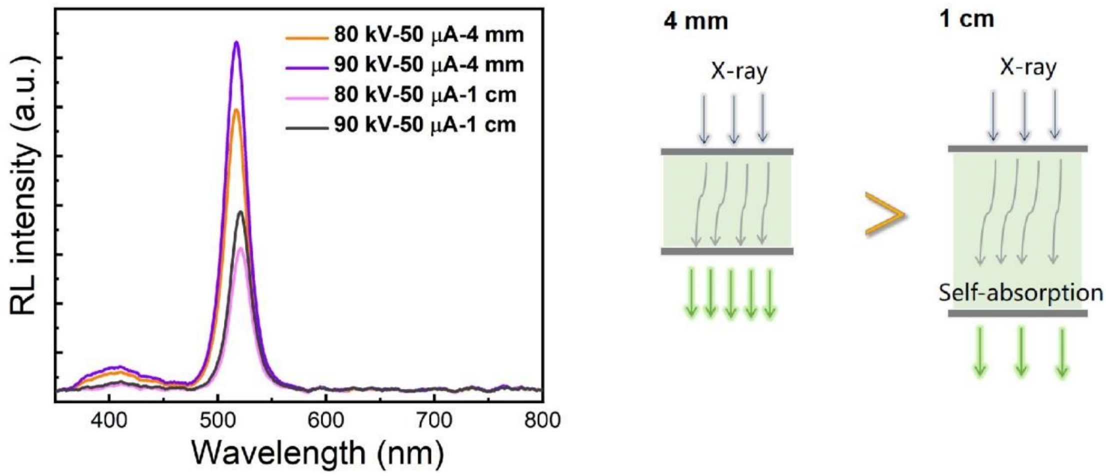

Figure S18 RL spectra of $CsPbBr_3$ QDs/PPO LSS with 4 mm and 1 cm thickness (80 kV-50 μA and 90 kV-50 μA).

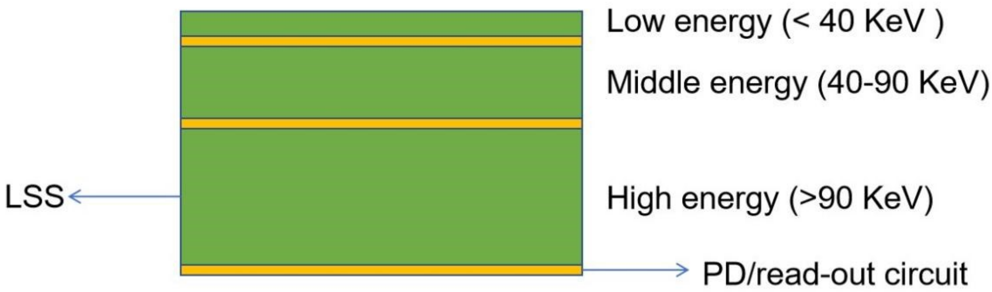

Figure S19 Schematic diagram of the energy resolved X-ray detector based on the LSS.

Table S1 Measured dose rate as the function of tube voltage and current.

Voltage-current	20 kV- 10 μA	20 kV- 20 μA	20 kV- 30 μA	20 kV- 40 μA	20 kV- 50 μA	20 kV- 60 μA	20 kV- 70 μA	20 kV- 80 μA	20 kV- 90 μA	20 kV- 100 μA
Dose rate (μGy/s)	15.25	29.72	44.17	58.61	73.33	88.89	102.78	119.44	130.56	144.63

Scintillator	Light yield (Photons/keV)	
CsI(TI) : Commercial Solid	54.0	473%
NaI(TI) : Commercial Solid	38.0	330%
Standard LS : PPO+POPOP+toluene	11.4	100%
Hybrid LS : $CsPbBr_3$ (60 mg/ml)+PPO (30 mg/ml)	9.6	84%
Hybrid LS : $CsPbBr_3$ (60 mg/ml)+PPO (60 mg/ml)	10.6	93%
$CsPbBr_3$ (60mg/ml)	3.0	27%

Table S2. Comparison of the light yield of various solid and liquid scintillators. The light yield of the standard PPO+POPOP+toluene is known, then the light yield values of other liquid scintillators were evaluated versus to that of the standard PPO+POPOP +toluene scintillator. The efficiency of the commerical CsI and NaI solid scintillator were obtained from Ref. (Tsipenyuk, Y. M. Physical methods, instruments and measurements, Volume II, p. 71).